Baumgardt, H, He, C, Sweet, SM, Drinkwater, M, Sollima, A, Hurley, J, Usher, C, Kamann, S, Dalgleish, HS, Dreizler, S and Husser, T-O

 No evidence for intermediate-mass black holes in the globular clusters ω Cen and NGC 6624

Article

For more information please contact researchonline@ljmu.ac.uk

No evidence for intermediate-mass black holes in the globular clusters ω Cen and NGC 6624

H. Baumgardt [©],[1]⋆ C. He,[1] S. M. Sweet [©],[2,3] M. Drinkwater [©],[1] A. Sollima [©],[4]
J. Hurley,[2] C. Usher [©],[5] S. Kamann [©],[5] H. Dalgleish [©],[5] S. Dreizler[6] and T.-O. Husser[6]

[1]*School of Mathematics and Physics, The University of Queensland, St Lucia, QLD 4072, Australia*
[2]*Swinburne University of Technology, PO Box 218, Hawthorn, Victoria 3122, Australia*
[3]*ARC Centre of Excellence for All-sky Astrophysics in 3 Dimensions (ASTRO 3D)*
[4]*INAF Osservatorio Astronomico di Bologna, via Gobetti 93/3, Bologna I-40129, Italy*
[5]*Astrophysics Research Institute, Liverpool John Moores University, 146 Brownlow Hill, Liverpool L3 5RF, UK*
[6]*Institute for Astrophysics, Georg-August-University, Friedrich-Hund-Platz 1, D-37077 G'ottingen, Germany*

ABSTRACT

We compare the results of a large grid of N-body simulations with the surface brightness and velocity dispersion profiles of the globular clusters ω Cen and NGC 6624. Our models include clusters with varying stellar-mass black hole retention fractions and varying masses of a central intermediate-mass black hole (IMBH). We find that an $\sim 45\,000$ $M_\odot$ IMBH, whose presence has been suggested based on the measured velocity dispersion profile of ω Cen, predicts the existence of about 20 fast-moving, $m > 0.5$ $M_\odot$, main-sequence stars with a (1D) velocity $v > 60$ km s^{-1} in the central 20 arcsec of ω Cen. However, no such star is present in the *HST*/ACS proper motion catalogue of Bellini et al. (2017), strongly ruling out the presence of a massive IMBH in the core of ω Cen. Instead, we find that all available data can be fitted by a model that contains 4.6 per cent of the mass of ω Cen in a centrally concentrated cluster of stellar-mass black holes. We show that this mass fraction in stellar-mass BHs is compatible with the predictions of stellar evolution models of massive stars. We also compare our grid of N-body simulations with NGC 6624, a cluster recently claimed to harbour a 20 000 $M_\odot$ black hole based on timing observations of millisecond pulsars. However, we find that models with $M_{\rm IMBH} > 1000$ $M_\odot$ IMBHs are incompatible with the observed velocity dispersion and surface brightness profile of NGC 6624, ruling out the presence of a massive IMBH in this cluster. Models without an IMBH provide again an excellent fit to NGC 6624.

Key words: stars: luminosity function, mass function – globular clusters: general.

1 INTRODUCTION

Black holes were long considered to be a mathematical curiosity, but nowadays their existence has firm observational support. Until recently, observational evidence for black holes has mainly been gathered in two distinct mass ranges: stellar-mass black holes, which are produced as the end product of the stellar evolution of massive stars (Fryer 1999), and supermassive black holes with masses 10^6–10^{10} $M_\odot$, which are found in the centres of galaxies (Gebhardt et al. 2000; Gültekin et al. 2009).

In recent years, evidence has also been accumulating for the existence of intermediate-mass black holes (IMBHs) with masses in the range 10^3–10^5 $M_\odot$. First, some IMBHs have been found in the centres of dwarf galaxies. Barth et al. (2004) for example found

a 10^5 $M_\odot$ black hole at the centre of the Seyfert 1 galaxy POX 52 through optical imaging and stellar radial velocity measurements. Farrell et al. (2009) found evidence that the ultraluminous X-ray source in the galaxy ESO243-49 is powered by an accreting black hole with mass 10^2–10^5 $M_\odot$. Further evidence for an IMBH nature of the accreting black hole was later found by Webb et al. (2010) and Servillat et al. (2011). Accreting IMBH candidates were also found at the centres of the galaxies NGC 404 (Nyland et al. 2012) and NGC 3319 (Jiang et al. 2018), making it plausible that IMBHs could be intermediate steps in the formation of supermassive black holes. Most recently Lin et al. (2018) found that a luminous X-ray outburst in a massive star cluster near the lenticular galaxy 6dFGS gJ215022.2-055059 was most likely powered by the tidal disruption of a star by a 50 000 $M_\odot$ IMBH.

IMBHs might also exist in globular clusters, created through either the formation of a central cluster of compact remnants that later merge due to the emission of gravitational waves (Miller &

⋆ E-mail: h.baumgardt@uq.edu.au

Hamilton 2002; Mouri & Taniguchi 2002), run-away merging of massive main-sequence stars within the first few Myrs after cluster formation (Portegies Zwart et al. 2004), or the repeated formation of tight binaries between a stellar-mass black hole and main-sequence stars followed by mass accretion on to the black hole and subsequent growth of the black hole over longer time-scales (Giersz et al. 2015). IMBHs might also be the remnants of ~10^4 M$_\odot$ supermassive stars that have been suggested as the sources of the observed abundance anomalies in globular clusters (Denissenkov & Hartwick 2014).

Observational evidence for the existence of IMBHs has been reported in about 20 Galactic globular clusters based on either stellar kinematics (e.g. Gerssen et al. 2002), X-ray or radio signals from accretion of interstellar gas (Ulvestad, Greene & Ho 2007) or the acceleration of pulsars (Kızıltan, Baumgardt & Loeb 2017; Perera et al. 2017a). In particular, Noyola, Gebhardt & Bergmann (2008), Jalali et al. (2012), and Baumgardt (2017) found evidence for a 40 000 M$_\odot$ IMBH in the centre of ω Cen based on the velocity dispersion and surface brightness profile of this cluster. Since ω Cen is thought to be the nuclear cluster of a tidally disrupted dwarf galaxy (e.g. Bekki & Norris 2006), such a discovery could provide a link between IMBHs and supermassive black holes. However, the presence of an IMBH in ω Cen was challenged by van der Marel & Anderson (2010), who created models of ω Cen that fitted the velocity dispersion profile of the cluster without the need for an IMBH, and by Zocchi, Gieles & Hénault-Brunet (2019), who fitted the velocity dispersion profile of ω Cen by a model that contained a centrally concentrated cluster of stellar-mass black holes. Furthermore, Haggard et al. (2013) found no evidence of radio signals from gas accretion on to a central black hole in ω Cen.

In addition, Perera et al. (2017a, b) found evidence for a massive IMBH in NGC 6624 based on timing observations of several pulsars close to the cluster centre. However, Gieles et al. (2018) were able to explain the observed period changes by a cluster model that did not contain an IMBH. In summary, there is currently no undisputed case for an IMBH in any Galactic globular cluster. If IMBHs exist in globular clusters, most of them must have masses of less than a few thousand M$_\odot$, otherwise their influence on the velocity dispersion profiles (Baumgardt 2017) or radio emission from the accretion of interstellar gas (Strader et al. 2012; Tremou et al. 2018) should have been detected.

In this paper, we use theoretical models to investigate whether the surface brightness and velocity dispersion profiles of the globular clusters ω Cen and NGC 6624 require the presence of IMBHs in these clusters. Our models are based on direct *N*-body simulations, which follow the evolution of both clusters under the combined influence of stellar evolution and two-body relaxation. For ω Cen we also investigate a centrally concentrated cluster of stellar-mass black holes as an alternative to an IMBH. Our paper is organized as follows. In Section 2, we describe the observational data used in this work. In Section 3, we describe the grid of *N*-body simulations used to fit the velocity and surface brightness profiles and the stellar-mass functions of globular clusters. In Section 4, we compare the *N*-body models with the observations and we draw our conclusions in Section 5.
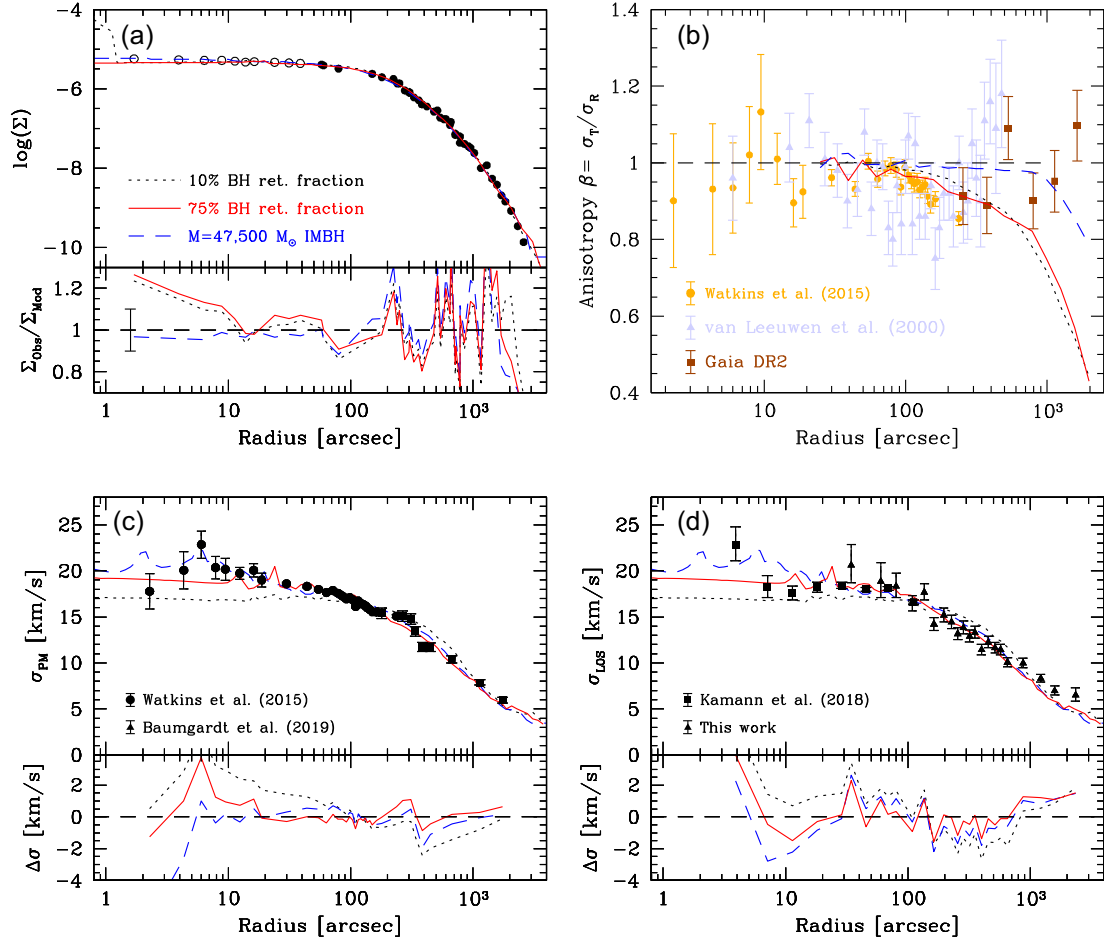
2 OBSERVATIONAL DATA

2.1 ω Cen

Our main source for the kinematic data on ω Cen are the radial velocity dispersion profiles recently published by Baumgardt (2017) and Baumgardt & Hilker (2018). Baumgardt (2017) calculated

the velocity dispersion based on ~4500 individual stellar radial velocities from published literature data, while Baumgardt & Hilker (2018) determined the radial velocities of an additional 1000 cluster stars from unpublished ESO/FLAMES spectra. In order to improve the coverage of the outer regions of ω Cen, we added to this data a set of 10 AAOmega/2dF observations of ω Cen made between 2007 July and 2011 May, that we downloaded from the AAT Data Archive. We restricted ourselves to AAOmega spectra taken with the 1700D grating that have a spectral resolution of $R = 10\,000$, the highest of all available AAOmega gratings. The basic data reduction of these spectra was done with the IRAF task 2dfdr, which also performed the heliocentric correction of the spectra. We calculated radial velocities from the reduced spectra with the help of the IRAF task fxcor, which is based on the Fourier cross-correlation method developed by Tonry & Davis (1979). For the cross-correlation, we used as template the spectrum of a cool giant star that we created with the help of the stellar synthesis program SPECTRUM (Gray & Corbally 1994) using ATLAS9 stellar model atmospheres (Castelli & Kurucz 2004) with a metallicity of [Fe/H] = −1.50 as input.

In total, we obtained 6500 radial velocities of stars in the field of ω Cen, from which we calculated the velocity dispersion profile of ω Cen using a maximum-likelihood approach. We first cross-correlated the different data sets against each other to bring them to a common mean radial velocity and cross-matched the stellar positions against the *Gaia* DR2 catalogue. We next removed all stars that have proper motions incompatible with the mean cluster motion determined by Baumgardt et al. (2019). The mean cluster velocity and velocity dispersion profile were then determined using all remaining stars and the membership probability of each star was determined based on the velocity dispersion of the cluster. We then removed stars with radial velocities differing by more than 3σ from the cluster mean from the sample and calculated a new mean cluster velocity and velocity dispersion profile. This procedure was repeated until a stable solution for the list of cluster members and the velocity dispersion profile was found and we reached this convergence within two or three steps.

In order to increase the coverage of the central cluster region, we also use the velocity dispersion profile published by Kamann et al. (2018) based on VLT/MUSE observations in our modelling. We accompany the line-of-sight radial velocity data with the *HST*-based proper motion dispersion profile of Watkins et al. (2015) in the inner cluster parts and the *Gaia* DR2 proper motion dispersion profile from Baumgardt et al. (2019). Finally, we use the catalogue of 240 000 stars with measured *HST* proper motions and photometry derived by Bellini et al. (2014) and Bellini et al. (2017). When transforming the proper motions into velocities, we assume a distance of $d = 5.24$ kpc to ω Cen (Baumgardt et al. 2019). The resulting velocity dispersion profile of ω Cen is shown in Fig. 1. It can be seen that the velocity dispersion is roughly constant in the central 100 arcsec, and decreases further out before levelling off beyond about 1000 arcsec. There is generally very good agreement between the *HST* proper motion based velocity dispersion profile and the line-of-sight radial velocities. Inside 10 arcsec both the line-of-sight radial velocity dispersion profile as well as the proper motion dispersion profile show some larger scatter due to a lack of stars with measured kinematics.

In addition to the velocity dispersion profile, we also fit the observed surface brightness profiles with our *N*-body models. For both ω Cen and NGC 6624, we create surface brightness profiles by combing the *HST* based surface brightness profile of Noyola & Gebhardt (2006) in the inner cluster parts with the ground-based

Figure 1. Fit of the surface brightness profile (panel a) and the velocity dispersion profile (panels c and d) of ω Cen for the best-fitting *N*-body models. Upper panels show the actual profiles, lower panels show the differences between the observed and modelled profiles. The surface brightness profile from Trager et al. (1995) is shown by solid circles, while open circles show the data from Noyola & Gebhardt (2006). The errorbar in the lower left of panel (a) depicts an uncertainty of 0.1 mag. In panels (c) and (d), the observed velocity dispersions are from Watkins et al. (2015) (circles), Kamann et al. (2018) (squares), and this work (triangles). Shown are the best-fitting IMBH model (blue dashed lines) and the best-fitting no-IMBH model with a retention fraction of stellar-mass black holes of 75 per cent (red solid lines). Also shown is the best-fitting model with a 10 per cent retention fraction of black holes (black dotted lines). All three models fit the surface brightness profile within the observational uncertainties outside the central 10 arcsec. The model with a low assumed retention fraction of stellar-mass black holes has too little mass in the centre and underpredicts the observed velocity dispersion in the centre and overpredicts it at larger radii. The model with a high stellar-mass black hole retention fraction provides a significantly better fit. Panel (b) compares the anisotropy profile of ω Cen with all three models. The models are in agreement with the observed profile out to several hundred arcsec.

data of Trager, King & Djorgovski (1995) at larger radii. The mass function of ω Cen has been measured by Sollima, Ferraro & Bellazzini (2007), who found a steep, Salpeter-like increase of the mass function between $0.5\,M_\odot < m < 0.8\,M_\odot$, a break in the mass function at $m = 0.5\,M_\odot$ and a flatter increase below this mass. Since this mass function is close to a Kroupa initial mass function, we use *N*-body models with a Kroupa mass function to model ω Cen. A mass function rich in low-mass stars is also reasonable, given the high mass and long relaxation time of ω Cen, which means that only little mass segregation and little dynamical mass-loss have occurred over a Hubble time.

2.2 NGC 6624

Radial velocities for 19 stars in the centre of NGC 6624 were determined by Pryor et al. (1991). In addition, Baumgardt & Hilker (2018) determined the radial velocities of 125 stars in the field of NGC 6624 based on archival VLT/FLAMES observations (proposal

ID: 083.D-0798(D), PI: B. Lanzoni) and another eight cluster stars from Keck/NIRSPEC observations (Keck proposal ID U17NS, PI: M. Rich). We add to this data set, 58 stars in the central region with measured radial velocities from the WAGGS survey (Usher et al. 2017). The observations were made using the WiFeS integral field spectrograph (Dopita et al. 2007, 2010) and the basic data reduction was done as described in Usher et al. (2017). Using PAMPELMUSE (Kamann, Wisotzki & Roth 2013), stellar spectra were extracted from the WAGGS data cubes and radial velocities were determined with the IRAF task fxcor. Further details will be described in a forthcoming paper (Dalgleish et al. in preparation). We furthermore added radial velocities based on MUSE observations of NGC 6624 that were taken during the nights of 2015-05-11 and 2017-10-17, as part of observing programmes 095.D-0629 and 0100.D-0161 (PI: Dreizler). The reduction and analysis of the data were performed as described in Kamann et al. (2018). In particular, we used PAMPELMUSE to extract stellar spectra from the reduced data cubes, while the derivation of the final radial velocities was done with

SPEXXY (see Husser et al. 2016). For the present study, we selected a high-quality sample of 241 stars with $V < 17$ and radial velocity uncertainties $< 1.5\,\mathrm{km\,s^{-1}}$ from the full MUSE sample for NGC 6624.

In order to increase the number of stars with measured radial velocities in the outer cluster parts, we also observed NGC 6624 for one half-night using the DEIMOS spectograph (Faber et al. 2003) on the Keck II telescope (Programm ID: Z252, PI: M. Drinkwater). Observations were performed on 2017 July 19 with 0.6 arcsec seeing and some thin cirrus, using the 1200G grating with a central wavelength of 8000 Å and the OG550 order-blocking filter. Four slitmasks were observed at position angles (PAs) of 0, 90, 270, and 315 deg, in order to maximize the number of stars near the centre of the cluster, where the proportion of member stars is expected to be higher, and to maximize the spatial coverage of the outer regions. Slits were placed on a total of 685 unique targets, comprised of 545 stars with 2MASS coordinates and 140 with positions derived from *HST* imaging. Each mask had seven stars in common with the VLT/FLAMES data set to assist in radial velocity calibration. Exposure times were 3 x 800 s for the mask with PA = 0, 3 x 850 s for PA = 270, and 3 x 900 s for the masks with PA = 90 and 315.

The DEIMOS spectra were reduced with the help of the DEEP2 data reduction pipeline developed by the DEEP2 survey team (Cooper et al. 2012; Newman et al. 2013). Individual stellar radial velocities were again determined from the reduced spectra with the help of the IRAF fxcor task. To correct for residual systematic errors in the absolute wavelength calibration of the DEIMOS spectra, we cross-correlated them against a telluric template spectrum that was kindly provided to us by Tony Sohn and Emily Cunningham. Since the telluric lines should be at zero radial velocity, wavelength calibration errors can be corrected from the radial velocity of these lines. Final radial velocities for each star were then calculated according to $v_r = v_{\mathrm{obs}} - v_{\mathrm{tel}} - v_{\mathrm{hel}}$, where v_{obs} is the radial velocity derived from the stellar template, v_{tel} the radial velocity from the telluric spectrum and v_{hel} the heliocentric correction. In total, we were able to determine the radial velocities of 264 stars from the DEIMOS spectra. Table A1 gives the individual radial velocities that we have derived from the DEIMOS spectra. The membership probabilities in Table A1 are calculated as described in Baumgardt & Hilker (2018).

Our final data set consists of about 600 stars with measured radial velocities in the field of NGC 6624, out of which about 200 stars are cluster members. 35 stars have measured radial velocities from both the VLT/FLAMES observations and our DEIMOS observations and 31 stars are in common between the MUSE data and the combined VLT/FLAMES and Keck/DEIMOS data set. Virtually all the stars measured by Pryor et al. as well as the stars measured by the WAGGS survey are also in the MUSE sample. The good overlap between the different data sets allows us to bring them to within 0.3 km s^{-1} of each other. Since the remaining uncertainty adds quadratically to the true velocity dispersion profile, it does not significantly influence our measurement of the final velocity dispersion profile.

In order to calculate the velocity dispersion profile of NGC 6624 from the individual stellar radial velocities, we again cross-correlated the different data sets against each other to bring them to a common mean radial velocity and then selected as possible cluster members all stars with radial velocities between 30 km s^{-1} $< v < 80$ km s^{-1} and *Gaia* DR2 proper motions that match the mean cluster proper motion determined by Baumgardt et al. (2019). Due to the significant stellar background density, we restricted the member search to distances less than 200 arcsec from the cluster centre, since outside this radius a reliable membership determination was not

Table 1. Observed line-of-sight velocity dispersion profiles of ω Cen and NGC 6624. For each bin, the table gives the name of the cluster, the number of stars used to calculate the radial velocity dispersion, the average distance of stars from the cluster centre, and the velocity dispersion together with the 1σ upper and lower errorbars.

Cluster	N_{RV}	r (arcsec)	σ (km s^{-1})	$\Delta\sigma_u$ (km s^{-1})	$\Delta\sigma_l$ (km s^{-1})
ω Cen	95	44.10	19.09	1.46	1.29
ω Cen	100	75.11	19.00	1.44	1.29
ω Cen	195	101.14	15.72	0.84	0.77
ω Cen	195	126.99	17.94	0.95	0.87
ω Cen	195	148.85	15.89	0.85	0.78
ω Cen	195	171.92	14.63	0.78	0.71
ω Cen	195	198.68	15.39	0.82	0.76
ω Cen	195	222.19	14.44	0.77	0.70
ω Cen	195	244.66	14.30	0.76	0.70
ω Cen	195	266.18	12.84	0.68	0.63
ω Cen	195	288.99	13.83	0.73	0.68
ω Cen	195	315.19	12.89	0.69	0.63
ω Cen	195	341.95	13.27	0.70	0.65
ω Cen	195	378.73	11.72	0.62	0.58
ω Cen	195	426.96	11.96	0.64	0.59
ω Cen	195	480.76	12.66	0.67	0.62
ω Cen	195	536.14	11.22	0.60	0.55
ω Cen	195	590.69	10.86	0.58	0.54
ω Cen	195	681.63	9.58	0.51	0.47
ω Cen	195	943.29	9.52	0.51	0.47
ω Cen	195	1279.52	8.32	0.45	0.41
ω Cen	120	1898.97	6.77	0.47	0.42
NGC 6624	46	4.33	6.41	0.75	0.63
NGC 6624	46	9.93	7.13	0.83	0.71
NGC 6624	46	15.15	6.15	0.72	0.61
NGC 6624	46	20.27	6.04	0.71	0.60
NGC 6624	46	26.54	5.11	0.60	0.51
NGC 6624	46	40.96	5.15	0.61	0.52
NGC 6624	50	95.83	3.25	0.39	0.32

possible. The calculation of the velocity dispersion profile was again done via a maximum-likelihood approach, following the procedure described above for ω Cen. The resulting velocity dispersion profile is presented in Table 1.

We also used the proper motion velocity dispersion profile of Watkins et al. (2015) who determined the velocity dispersion profile inside 80 arcsec based on ∼1800 stars with magnitudes brighter than about 1.5 mag below the main-sequence turn-off. We finally used the stellar-mass function of NGC 6624 measured by Saracino et al. (2016) in the central 40 arcsec from ultra-deep, adaptive optics assisted J and K_S band Gemini/GSAOI images to constrain the mass function of the best-fitting *N*-body models.

3 *N*-BODY MODELS

We used the grid of *N*-body simulations presented by Baumgardt (2017) and Baumgardt & Hilker (2018) to model ω Cen and NGC 6624 and to derive limits on the presence of IMBHs in these clusters. Baumgardt (2017) and Baumgardt & Hilker (2018) have run a grid of 1400 *N*-body simulations of star clusters containing $N = 100\,000$ or $N = 200\,000$ stars using NBODY6 (Aarseth 1999; Nitadori & Aarseth 2012), varying the initial density profile and half-mass radius, the initial mass function, the cluster metallicity, and the mass fraction of an IMBH in the clusters. All models consisted initially only of single stars and formed binaries only through encounters of

stars in the cluster centres. Given the low observed binary fraction in globular clusters [only of order 10 per cent, see e.g. Milone et al. (2012) and Ji & Bregman (2013)], we do not think that our results would significantly change with the inclusion of primordial binaries. The basic strategy that we use to compare the *N*-body models with the observed surface brightness and velocity dispersion profile of a globular cluster is the same as in these two papers and we refer the reader to these papers for a detailed description. In short, the *N*-body simulations were run up to an age of $T = 13.5$ Gyr and final cluster models were calculated by taking 10 snapshots from the simulations centred around the age of each globular cluster. The combined snapshots of the *N*-body clusters were then scaled in mass and radius to match the density and velocity dispersion profiles of the observed globular clusters and the best-fitting model was determined from an interpolation in the grid of *N*-body models. When comparing with the *N*-body data, we assume an age of $T = 11.25$ Gyr for NGC 6624 (VandenBerg et al. 2013) while for ω Cen we assume an age of $T = 12.0$ Gyr. Our results are however not very sensitive to the adopted cluster age.

In order to model ω Cen, we ran an additional grid of models in which we varied the retention fraction of stellar-mass black holes. The simulations by Baumgardt (2017) and Baumgardt & Hilker (2018) assume a retention fraction of 10 per cent for the black holes that form in the simulations, with the remaining black holes given such high kick velocities upon formation that they immediately leave the star clusters. Such a retention fraction could be too small for ω Cen, since the models by Baumgardt & Hilker (2018) predict a central escape velocity of $v_{esc} = 63$ km s^{-1} for ω Cen, which is one of the highest central escape velocities of all Galactic globular clusters. Given that the initial escape velocity was probably even higher due to stellar evolution driven mass-loss and cluster expansion, a significant fraction of black holes could have been retained in ω Cen. In this paper, we therefore ran additional simulations of star clusters without IMBHs, but with stellar-mass black hole retention fractions of 30 per cent, 50 per cent, and 100 per cent. The initial mass function of stars in these simulations was also assumed to be a Kroupa (2001) mass function initially.

We also ran additional simulations for NGC 6624, since the IMBH models of Baumgardt (2017) only contain IMBHs with up to 2 per cent of the cluster mass at $T = 12$ Gyr, while the 20 000 M$_\odot$ IMBH inferred by Perera et al. (2017a, b) implies a much larger mass fraction. We therefore extended the grid of IMBH models of Baumgardt (2017) to also contain IMBH masses of 5 per cent and 10 per cent of the final cluster mass.

4 RESULTS

4.1 ω Cen

We start our discussion of ω Cen by comparing the best-fitting *N*-body models with and without an IMBH to the observed surface brightness and velocity dispersion profile of ω Cen. Three sets of models were calculated. In the first set of models, we kept the black hole retention fraction fixed at 10 per cent and varied only the initial cluster radius and the initial surface brightness profile, quantified by the King concentration parameter c. This was done until we found the best-fitting model to the observed surface brightness and velocity dispersion profile. These models are the same models as the *N*-body models used by Baumgardt (2017) and Baumgardt & Hilker (2018). When scaled to ω Cen, these models produce about 34 000 M$_\odot$ in stellar-mass black holes after stellar evolution and velocity kicks have been applied, out of which 14 000 M$_\odot$ remain

in the cluster by $T = 12$ Gyr. In the second set of models, we varied the assumed black hole retention fraction in addition to the initial cluster radius r_h and initial surface density profile. In the third set of models, we fixed the retention fraction of stellar-mass black holes to 10 per cent, but varied the mass fraction of a central IMBH from 0.5 per cent to 2 per cent of the final cluster mass, corresponding in the case of ω Cen to IMBHs with masses between about 12 000 and 50 000 M$_\odot$, to find the best fit to the observed surface brightness and velocity dispersion profile.

Fig. 1(a) shows the resulting fits of the surface brightness and velocity dispersion profile of ω Cen. Based on the differences between the polynomial fit of the surface brightness profile by Trager et al. (1995) and the actual surface brightness measurements, we estimate a typical uncertainty of the observed surface brightness of ω Cen of $\Delta\Sigma = 0.1$ mag. This uncertainty is shown in the lower left-hand panel of Fig. 1(a). It can be seen that all models provide fits of similar accuracy to the surface brightness profile of ω Cen, at least outside the central 10 arcsec. Inside this radius, the IMBH model provides a better fit to the weak cusp that Noyola & Gebhardt (2006) found in the surface brightness profile. We note however that several determinations of the centre of ω Cen exist and that Anderson & van der Marel (2010) did not find a rise in the surface brightness profile of ω Cen around their centre. We conclude that the surface brightness profile alone cannot be used to discriminate between the different models. The main reason for this is the low central concentration and long relaxation time of ω Cen, which means that the cluster is still far from core collapse and has not undergone much dynamical evolution. Such evolution would be necessary to establish a weak cusp profile in the surface brightness profile, which would separate models with and without IMBHs from each other (see discussion in Baumgardt, Makino & Hut 2005).

Figs 1(c) and (d) compare the velocity dispersion profiles predicted by the different models against the proper motion and radial velocity dispersion profile of ω Cen. It can be seen that the model with an initial retention fraction of stellar-mass black holes of 10 per cent (about 14 000 M$_\odot$ in stellar-mass black holes after $T = 12$ Gyr) underestimates the velocity dispersion in the central 100 arcsec by about 2 km s^{-1}. It also overpredicts the velocity dispersion profile beyond 200 arcsec and can therefore be rejected. The best-fitting model in which the black hole retention fraction and the total mass in stellar-mass black holes was left as a free parameter is shown by a solid, red line in Fig. 1. For an initial retention fraction of stellar-mass black holes of 75 per cent $\pm$ 8 per cent (corresponding to 165 000 M$_\odot$ or about 4.6 per cent $\pm$ 0.5 per cent of the cluster mass in stellar-mass black holes at $T = 12$ Gyr), this model provides a significantly better fit to the velocity dispersion profile, especially in the inner cluster parts. Due to mass segregation of the stellar-mass black holes into the centre, the mass in the centre is increased compared to the model with a low retention fraction and this increases the velocity dispersion of the stars. Similarly, a model with a $M_{IMBH} = 47\,500$ M$_\odot$ IMBH provides a good fit to the velocity dispersion profile. Our results confirm the models of Zocchi et al. (2019) who already found that a dense cluster of stellar-mass black holes containing 5 per cent of the total cluster mass can mimic the influence of an IMBH.

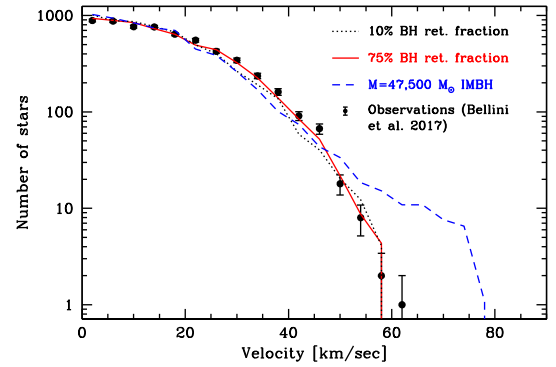#### 4.1.1 Central velocity distribution

Fig. 2 shows the 1D velocity distribution in the centre of ω Cen for the different *N*-body models and compares them with the observed velocity distribution which we calculated from the proper motion

data published by Bellini et al. (2017). For the observed profile, we used all stars within a projected radius of 20 arcsec of the cluster centre as determined by Goldsbury, Heyl & Richer (2013). This area is large enough to encompass the cluster centres of Noyola & Gebhardt (2006) and van der Marel & Anderson (2010) as well, which are about 12 and 0.5 arcsec, respectively, away from the Goldsbury et al. cluster centre. We restrict ourselves to stars that have reduced χ_r^2 values of less than 1.5, have a $N_{\rm Used}/N_{\rm found}$ ratio between the number of data points used for PM fits $N_{\rm Used}$ to the number of data points available $N_{\rm found}$ of larger than 0.85, proper motion errors of less than 5 km s^{-1}, and have velocities within 100 km s^{-1} of the mean cluster velocity. For the *N*-body models we use all main-sequence and giant stars that are more massive than 0.5 M$_\odot$ to roughly cover the same mass range as the stars with observed proper motions in the Bellini et al. sample. We scale all theoretical distributions to contain the same number of stars as are in the observed sample. We also add random velocity errors that follow a Gaussian with a width of 3 km s^{-1} to the stars from the *N*-body simulations to mimic the influence of velocity errors in the observations.

It can be seen that the model without an IMBH but a high black hole retention fraction matches the observed velocity distribution very well. In both data sets, the fastest star is moving with about 62 km s^{-1} and the overall shape of the observed velocity distribution is also matched very well. A Kolmogorov–Smirnov (KS) test between the theoretical and observed data gives a 15 per cent chance that both distributions are drawn from the same underlying distribution. Given the considerable uncertainties in e.g. the mass distribution of formed black holes, and the large number of observed stars in Fig. 1, which makes modelling their exact distribution challenging, we consider the black hole models to be in very good agreement with the observations. In contrast, the best-fitting IMBH model leads to a significantly less satisfactory fit of the velocity distribution. The stellar distribution extends to too high velocities, the IMBH model predicts 20 stars with velocity $v > 62$ km s^{-1}, while none is seen in the observations. The reason for the larger number of stars with very high velocities is the lowering of the central potential well due to the IMBH, which is more effective than that caused by a more widely distributed population of stellar-mass black holes. The absence of fast moving stars in the observations cannot be a selection effect, since such stars are present outside the central 20 arcsec and are most likely non-members that move with a large velocity relative to the cluster. The velocity distribution for a central IMBH also clearly deviates from the observed distribution at smaller velocities, and a KS test gives a less than 10^{-7} chance that both distributions are drawn from the same underlying distribution. The model with a low black hole retention fraction also does not match the observed distribution of slow moving stars. We therefore conclude that ω Cen does not contain an IMBH, or at least, if the cluster contains an IMBH, then its mass must be significantly less than the 47 500 M$_\odot$ needed to explain the velocity dispersion profile. Additional simulations with lower IMBH mass fractions and varying stellar-mass black hole fractions would be needed to determine the upper mass limit of an IMBH.

4.1.2 The role of anisotropy and rotation

Zocchi, Gieles & Hénault-Brunet (2017) investigated the influence of orbital anisotropy on the velocity dispersion profile of ω Cen by fitting `limepy` models (Gieles & Zocchi 2015) with varying degrees of radial anisotropy to the surface and velocity dispersion

Figure 2. Velocity distribution of stars within 20 arcsec of the centre of ω Cen. Shown is the 1D velocity distribution for the stars with measured proper motions by Bellini et al. (2017) (black dots) and the best-fitting *N*-body model with an IMBH (blue dashed line) and with 10 per cent and 75 per cent BH retention fractions (black dotted and red solid lines). The model with a high retention fraction of stellar-mass black holes provides the best fit to the observed distribution. The IMBH model predicts about 20 high-velocity stars with $v > 62$ km s^{-1} while none is seen in the observations. The velocity distribution of the IMBH and low black hole retention fraction models also have the wrong shape for stars moving with less than 60 km s^{-1}.

profile of the cluster. They found that the central velocity dispersion increases with increasing orbital radial anisotropy and that `limepy` models could be constructed that reproduced the proper motion dispersion profile of ω Cen without the need to invoke an IMBH in the centre of the cluster. While a massive IMBH is already ruled out by the velocity distribution of stars in the centre, orbital anisotropy might still have an influence on the parameters of the best-fitting models, especially the amount of stellar-mass black holes needed to reproduce the velocity dispersion profile.

Fig. 1(b) compares the orbital anisotropy profile of ω Cen with the velocity dispersion profile for the best-fitting model with a 10 per cent retention fraction of black holes, the best-fitting model with a higher black hole retention fraction and a model with a central IMBH. We define as orbital anisotropy the ratio of the tangential to the radial velocity dispersion component of the proper motions $\beta = \sigma_t/\sigma_r$. The observed anisotropy β is taken from the measurements of Watkins et al. (2015) and van Leeuwen et al. (2000). In addition, we determine the velocity anisotropy in the outer parts of ω Cen from the `Gaia` DR2 proper motions. The velocity distribution of stars in ω Cen is isotropic in the centre out to about 100 arcsec, slightly radially anisotropic with $\beta = 0.9$ at intermediate radii, before becoming more or less isotropic again in the outermost parts. The amount of anisotropy is overall rather small, with the tangential velocity dispersion σ_t never differing by more than 10 per cent from the radial velocity dispersion σ_r.

In the simulated clusters the velocity profile is also isotropic in the centre before becoming increasingly anisotropic beyond 100 arcsec due to stars being scattered out of the centre on to radial orbits. The simulated clusters provide an acceptable fit to the anisotropy profile in the inner parts but, except for the IMBH model which is isotropic out to about 1000 arcsec, are too anisotropic beyond about 400 arcsec. The increasing anisotropy is most likely due to the fact that the simulated clusters are isolated, while the Galactic tidal field deflects stars on their orbits inside ω Cen and keeps the cluster isotropic. This mismatch could be the reason why the velocity dispersion in the simulated clusters is below the observed velocity dispersion in the outermost parts of ω Cen. However, given
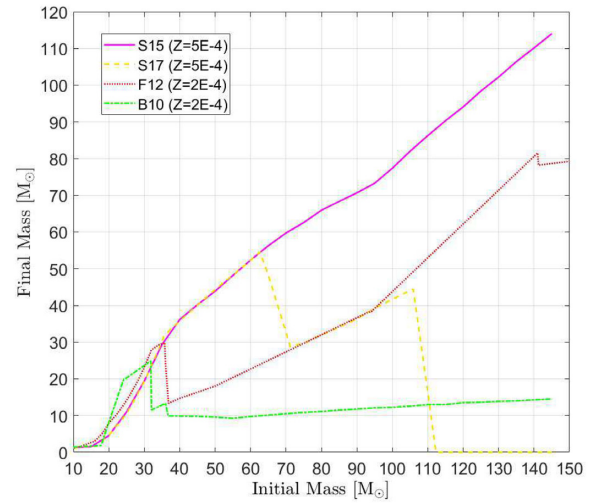
the good match in the centre, it seems quite unlikely that velocity anisotropy has a significant effect on our results.

In addition to anisotropy, rotation could also influence the results of our fitting since it re-distributes kinetic energy between different spatial directions while the models that we fit to ω Cen are non-rotating. Kamann et al. (2018) found a rotation amplitude of about 4 km s^{-1} in the central parts of ω Cen from MUSE spectroscopy. Similarly, Sollima, Baumgardt & Hilker (2019) found a rotational amplitude of $A = 4.27 \pm 0.52 \text{ km s}^{-1}$ and a 100 per cent probability that ω Cen is rotating by analysing the `Gaia` DR2 proper motions and stellar radial velocities of Baumgardt et al. (2019). Both values are significantly smaller than the central velocity dispersion, meaning that the influence of rotation is small in the centre It is therefore also unlikely that rotation has a significant influence on the derived black hole mass fraction and the possible presence of an IMBH. Finally, stellar binaries could also affect our velocity dispersion estimates. However, the binary fraction in ω Cen is small, only about 13 per cent (Sollima et al. 2007) and, according to the simulations by Ibata et al. (2011), the velocity shift of most of these binaries will be close to zero with only few systems producing velocity shifts larger than 20 km s^{-1}.

4.1.3 Implication for the initial stellar-mass black hole retention fraction

In this section, we compare the 4.6 per cent mass fraction in stellar-mass black holes that produced the best fit to the observational data of ω Cen with the estimated BH mass fraction predicted by stellar evolution theory. To this end, we set up an initial model of ω Cen assuming the cluster stars follow a Plummer model with an initial total cluster mass of $M = 7 \times 10^6 \text{ M}_\odot$ and initial half-mass radius of $r_h = 5$ pc, a Kroupa (2001) initial mass function between mass limits of 0.1 and $120 \text{ M}_\odot$ for the cluster stars and no primordial mass segregation between high- and low-mass stars. We then apply the effect of stellar evolution to this model by decreasing the masses of the stars and turning the more massive stars into compact remnants and evolve all stars to $T = 12$ Gyr. We also apply velocity kicks to the stars that turn into black holes.

We assume that stars with masses less than $0.8 \text{ M}_\odot$ do not undergo stellar evolution and keep their initial masses. Stars with initial masses between $0.8 < m < 8 \text{ M}_\odot$ are assumed to be transformed into white dwarfs and we use the initial-final mass function of Kalirai et al. (2008) to predict their masses. For the neutron stars, we assume that 90 per cent are removed due to natal kicks, in agreement with the assumption in the N-body models and that the mass of each neutron star is $m_{NS} = 1.3 \text{ M}_\odot$. For stellar-mass black holes, we test four different initial-final mass relations from the literature: Belczynski et al. (2010, B10), Fryer et al. (2012, F12), Spera, Mapelli & Bressan (2015, S15), and Spera & Mapelli (2017, S17). For the S15 and S17 models, we assume a cluster metallicity of $Z = 0.0005$, close to the average metallicity of ω Cen according to Harris (1996) and Johnson & Pilachowski (2010), while for the B10 and F12 models, we assume a metallicity of $Z = 0.0002$, which is the metallicity closest to the metallicity of ω Cen that was studied in detail in these papers. Fig. 3 depicts the final mass of a black hole versus the initial mass of a star for the four stellar evolution models and the metallicities chosen. We note that the initial-final mass relation for black holes in our N-body simulations is given by Belczynski, Kalogera & Bulik (2002), which is similar to the B10 and (for low stellar masses) F12 models, so these models can most easily be compared with the results of our simulations.

Figure 3. Final mass of a black hole as a function of the initial stellar mass for the stellar evolution models of B10, F12, S15, and S17. It can be seen that there is a significant variation between the four models especially for stars with mass $m > 30 \text{ M}_\odot$.
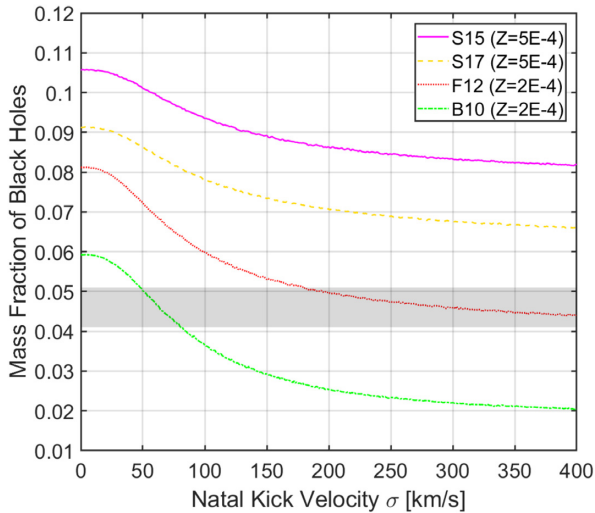
We also apply velocity kicks to the black holes. Following F12, we assume that the 1D kick velocity v_{kick} is given by the following formula:

$$v_{kick} = (1 - f_{fb})\,\sigma. \tag{1}$$

Here, f_{fb} is the mass fraction of the stellar envelope falling back onto the black hole (F12). We assume that σ, the 1D kick velocity in case of no mass fallback, follows a Gaussian distribution and we vary it between $0 < \sigma < 400 \text{ km s}^{-1}$ to explore the influence of σ on our results. We calculate three kick velocities for each spatial direction and add them to the velocity of the progenitor star upon formation of a black hole. Black holes are assumed to escape if their total energy is larger than zero and we sum up the masses of all remaining black holes to obtain the number and mass fraction of all black holes after their formation. Since the best-fitting N-body model of ω Cen loses about 1/3 of all black holes between the time of their formation and $T = 12$ Gyr due to dynamical encounters between single black holes and black hole binaries in the core of the cluster, we finally reduce the mass in stellar-mass black holes that we derive from the different stellar-evolution models by 1/3 in order to account for the dynamical mass-loss.

Fig. 4 depicts the mass fraction in stellar-mass black holes after 12 Gyr for the four different stellar evolution models. The black hole mass fraction decreases with increasing kick velocity but becomes roughly constant beyond 300 km s^{-1} due to black holes forming from stars with $f_{fb} \approx 1$ which receive only small kicks. The grey shaded area shows the observed fraction of 4.6 ± 0.5 per cent. It can be seen that the observed mass fraction is compatible with the B10 models for kick velocities up to about 80 km s^{-1} and with the F12 models for larger kick velocities. The F12 models produce the right black hole mass fraction for the 1D kick velocity of $\sigma = 270 \text{ km s}^{-1}$ found by Repetto et al. (2012) from observations of Galactic black holes. The S15 and S17 models overpredict the mass fraction of black holes due to the fact that more massive black holes form in these models, especially for high-mass stars. There are however several ways that could also bring these models into agreement with the observations, for example a steepening of the high-mass end of the initial mass function. In addition, the larger number of massive black holes that are produced in these models could lead

Figure 4. Black hole mass fraction after $T = 12$ Gyr as a function of the kick velocities σ for the four stellar evolution models depicted in Fig. 3. The grey shaded area shows the predicted black hole mass fraction in ω Cen from our N-body models. The current BH mass fraction is compatible with the F12 stellar evolution models and a 1D kick velocity of 270 km s^{-1} as found by Repetto, Davies & Sigurdsson (2012) or the B10 models for low kick velocities.

to a more efficient dynamical ejection of stellar-mass black holes, which could help to bring these models into better agreement with the observations. We therefore conclude that the mass fraction of stellar-mass black holes that we found from the N-body models is, within the model uncertainties, in agreement with the expected fraction based on recent models for the evolution of massive stars.

4.2 NGC 6624

Peuten et al. (2014) analysed 16 yr of timing data of the low-mass X-ray binary (LMXB) 4U 1820-30 that is located close to the centre of NGC 6624 and found that this LMXB has a strongly negative period derivative. They suggested that an acceleration of the star along the line of sight due to either a dark concentration of remnants or an IMBH could be responsible for creating this period change. Furthermore, Perera et al. (2017a) analysed timing observations of the three innermost pulsars in NGC 6624 and concluded that a 60 000 M$_\odot$ IMBH (later revised down to 20 000 M$_\odot$ by Perera et al. 2017b) is required if their period changes are due to a central IMBH. Gieles et al. (2018), on the other hand, noticed that the strong negative period derivative of 4U 1820-30 is not exceptional when compared to field LMXBs, making it likely that other explanations like mass-loss from the companion star or spin-orbit coupling can also explain the period change. They also showed through fitting of the observed surface brightness and velocity dispersion profile of NGC 6624 by multimass models that models without an IMBH are sufficient to explain the observed acceleration of pulsar A in NGC 6624.
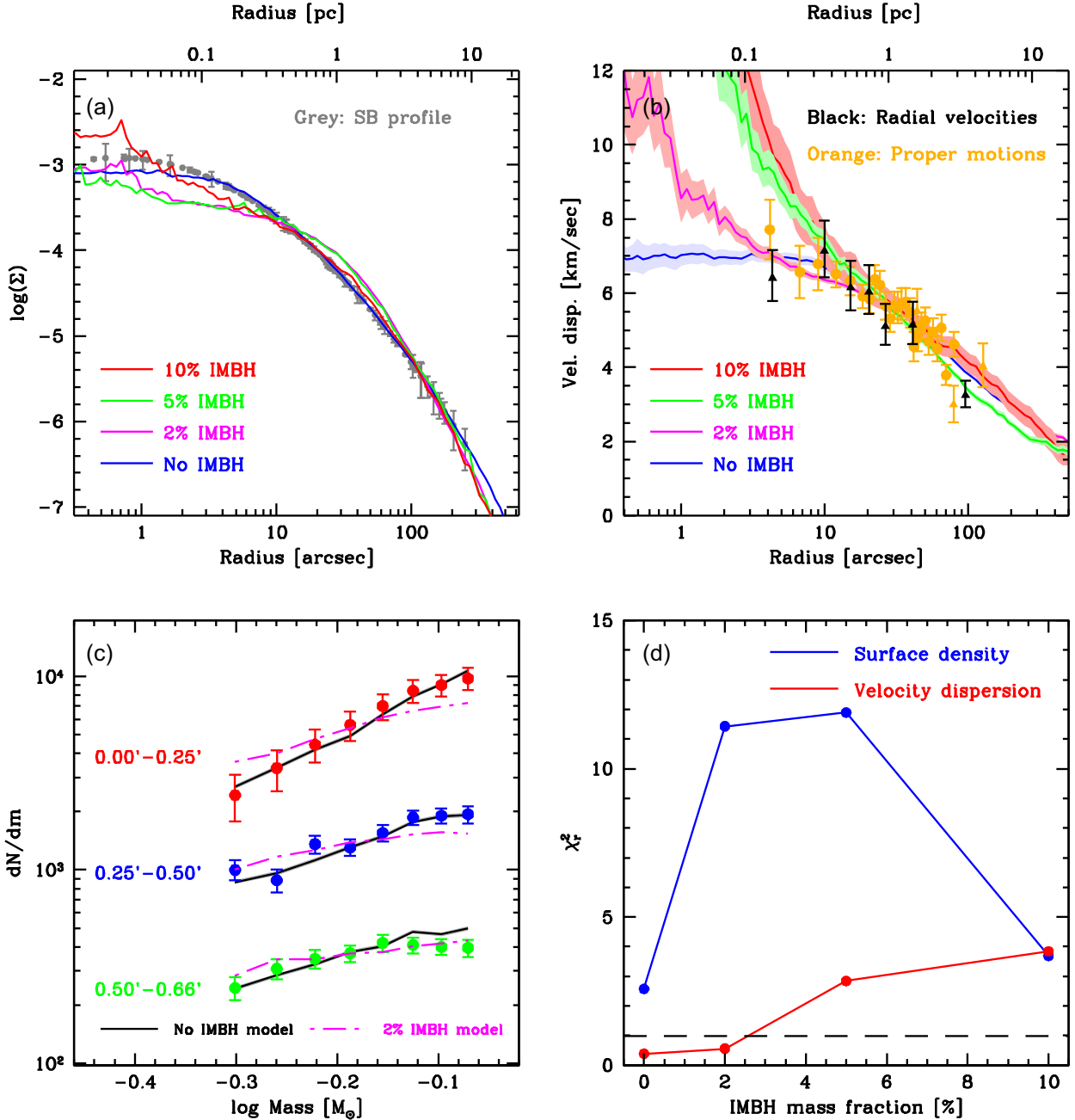
For a total cluster mass of 55 400 ± 1500 M$_\odot$ (Baumgardt & Hilker 2018; Baumgardt et al. 2019), even the lower IMBH mass of 20 000 M$_\odot$ of Perera et al. (2017b) would still imply that the IMBH would contain more than 1/3 of the total mass of NGC 6624, making NGC 6624 one of the most black hole dominated stellar systems known. We therefore also fitted our grid of N-body simulations to NGC 6624. Fig. 5 depicts cluster fits with various IMBH mass fractions to the observed velocity dispersion and surface brightness

profile of NGC 6624. We performed one set of simulations of clusters without a central black hole, and three sets of simulations of star clusters containing central black holes containing 2 per cent, 5 per cent and 10 per cent of the total cluster mass. For each IMBH mass fraction, we searched for the model that produced the best fit to the observed surface brightness and velocity dispersion profile of NGC 6624. It can be seen that the model without an IMBH is in excellent agreement with the observations, since it fits the observed surface brightness and velocity dispersion profile. There is a slight discrepancy with the observed surface density profile in the innermost few arcsec; however, this discrepancy is nowhere larger than a factor of 2 and is probably within the uncertainties with which the density profile can be determined in the centre.

Our N-body simulations therefore confirm earlier results by Gieles et al. (2018) who also found that no-IMBH is required to explain the observed surface brightness and velocity dispersion profile of NGC 6624. Models with IMBHs containing less than 5 per cent of the cluster mass in the form of an IMBH also provide acceptable fits to the velocity dispersion profile. However, more massive IMBH models start to overpredict the central velocity dispersion. Although we were not able to run models with IMBHs containing more than 10 per cent of the cluster mass in the form of an IMBH due to stability issues in the simulation, it is clear from Fig. 5 that such models would be excluded even more strongly. In addition all IMBH models produce weak cusps in the cluster centre that are in disagreement with the observed surface brightness profile. Finally, the IMBH models produce a smaller amount of mass segregation among the cluster stars than the no-IMBH model, which is unable to reproduce the strong change of the observed mass function with radius (see panel c). This reduced amount of mass segregation is in agreement with theoretical expectations (Baumgardt, Makino & Ebisuzaki 2004; Gill et al. 2008) and further argues against the presence of an IMBH in NGC 6624. We derive an upper limit for an IMBH in NGC 6624 of at most a few per cent (i.e. about 3000 M$_\odot$) if only the cluster kinematics is taken into account. This value drops to around 1000 M$_\odot$ if the fit of the surface brightness profile is also taken into account.

Table 2 presents the derived parameters for NGC 6624 from our best-fitting no-IMBH model. The cluster distance was determined by a simultaneous fit of the radial velocity dispersion and proper motion dispersion profiles. The global mass function slope α (defined as the best-fitting power-law slope $N(m) \sim m^\alpha$) was derived for main-sequence stars between 0.2 and 0.8 M$_\odot$. Its strongly positive value shows that the number of stars is decreasing towards lower masses, meaning that NGC 6624 is highly depleted in low-mass stars. For the best-fitting cluster distance, the mass-to-light ratio of NGC 6624 is around 1.4, somewhat below the expected M/L ratio of a cluster with a Kroupa IMF (around 1.7 given the age and metallicity of NGC 6624). This can be explained by the highly depleted mass function of NGC 6624. Our values for the total cluster mass, mass-to-light ratio and half-mass radius are in good agreement with those derived by Gieles et al. (2018).

Table 2 also presents the maximum accelerations for the LMXB and the three pulsars with measured period derivatives that are possible in the best-fitting model. The maximum accelerations were determined for stars at the same projected distance as each of the observed pulsars by varying the distance along the line of sight until the maximum line-of-sight acceleration was found. The central density of our best-fitting no-IMBH model is lower than the one found by Gieles et al. (2018). As a result, the observed period changes of the pulsars and the LMXB cannot be explained by our N-

Figure 5. Surface density profiles (panel a), velocity dispersion profiles (panel b), and stellar mass functions (panel c) of the best-fitting cluster models with and without an IMBH (blue lines) and the observed profiles of NGC 6624. Panel (c) shows the measured mass functions at three different radii. Only the comparison with the no-IMBH model is shown here for clarity. Panel (d) depicts the reduced χ_r^2 values for the fits of the different models against surface brightness and velocity dispersion profiles. While the cluster model without an IMBH is in good agreement with the observed cluster, none of the IMBH models provides a simultaneous fit of the observed surface brightness and velocity dispersion profile.

body model through an acceleration due to the smooth background cluster potential. Instead, they have to be either due to nearby stars or an internal spin-down of the pulsars. Indeed, the period derivative, $\dot{P}$, values of pulsars B and C are comparable with observed $\dot{P}$ values of field pulsars of similar period. These pulsars were also not considered by Perera et al. (2017b) for the determination of the cluster potential and IMBH mass. Pulsar A is the most luminous γ-ray pulsar known and the observed γ-ray luminosity requires an intrinsic period derivative that is comparable to the observed value (Freire et al. 2011).

A final caveat to note is that the results of our *N*-body fitting show that NGC 6624 has a half-mass relaxation time of around 10^8 yr, much smaller than its age, making it likely that NGC 6624 has gone through core-collapse. Clusters in core-collapse go through core oscillations during which the core continuously collapses and re-expands due to dynamical heating of the core due to binaries formed during the dense collapse phases (Bettwieser & Sugimoto 1984). This could significantly change the central density without affecting the outer density profile much, i.e. such density fluctuations might not be visible observationally. We therefore investigate how the

Table 2. Properties of NGC 6624 and observed and predicted accelerations of the millisecond pulsars from our best-fitting no-IMBH model.

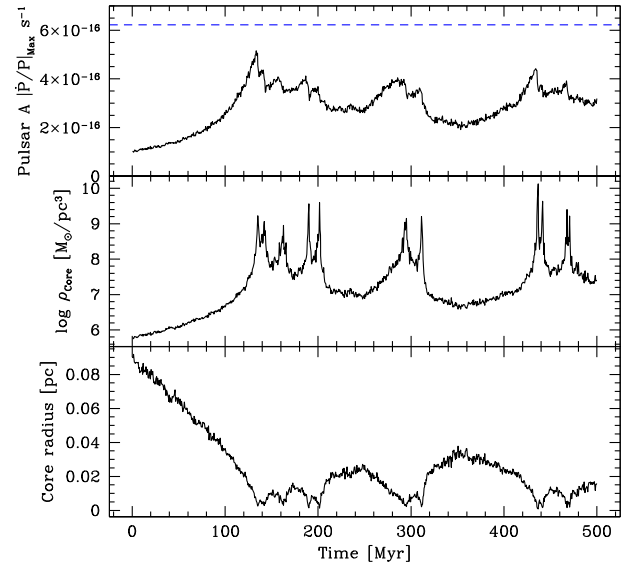|	
Distance	7425 ± 273 pc
Mass	$9.40 \pm 0.23 \times 10^4$ M$_\odot$
M/L ratio	1.37 ± 0.17 M$_\odot$/L$_\odot$
Mass function slope α	$+1.5$
Relaxation time T_{RH}	3.0×10^8 yr
Core radius	0.25 pc
Half-mass radius	2.50 pc
Central velocity dispersion	7.1 km s^{-1}
Half-mass density	7.3×10^2 M$_\odot$ pc^{-3}
Central density	6.1×10^5 M$_\odot$ pc^{-3}
Observed period derivatives $\dot{P}/P$	
PSR B1820-30A[1]	6.22×10^{-16} s^{-1}
PSR B1820-30B[1]	8.32×10^{-17} s^{-1}
PSR J1823-3021C[1]	5.51×10^{-16} s^{-1}
4U 1820-30[2]	-1.7×10^{-15} s^{-1}
Maximum accelerations	
PSR B1820-30A	1.03×10^{-16} s^{-1}
PSR B1820-30B	1.21×10^{-17} s^{-1}
PSR J1823-3021C	2.19×10^{-17} s^{-1}
4U 1820-30	8.79×10^{-17} s^{-1}

Note. 1: from http://www.naic.edu/ pfreire/GCpsr.html, 2: from Peuten et al. (2014).

previous results change over time. Fig. 6 shows the variation of the core radius, central density, and maximum acceleration of pulsar A in an *N*-body simulations that uses our best-fitting no-IMBH model as a starting point. This run was done without stellar evolution; however, we do not expect that stellar evolution will change the results significantly over the 500 Myr time-scale depicted in Fig. 6. The core radius and central density are calculated according to equation 2 of Baumgardt, Hut & Heggie (2002).

The model cluster quickly collapses and reaches a central density of around 10^9 M$_\odot$ pc^{-3}, three orders of magnitudes larger than the initial density of the best-fitting *N*-body model, after about $T = 130$ Myr of evolution. We note that the best fit to the surface density profile of NGC 6624 determined by Trager et al. (1995), which we use in this paper, is reached at about $T = 50$ Myr in this simulation, while the surface density profile determined by Gieles et al. (2018) corresponds to the density profile reached in the deepest collapse phases. After the initial collapse, core oscillations are clearly visible in the evolution of the core density and the central density can fluctuate by about two orders of magnitude within a few 10s of Myr. However, while the core can reach extremely high central densities, it contains only of order 30 stars during the densest collapse phases. As a result the maximum acceleration of a pulsar seen in projection at the same distance as pulsar A fluctuates much less and is always a factor 2–3 below the observed acceleration. We therefore conclude that the observed period change of pulsar A must at least in part be due to an internal period change or a nearby companion. It cannot solely be explained by an acceleration due to the general cluster potential, making this pulsar and also the other two pulsars unsuitable for the determination of the cluster potential and the presence of an IMBH in NGC 6624.

5 CONCLUSIONS

We have fitted results of dynamical *N*-body simulations to the surface brightness and velocity dispersion profiles of ω Cen and

Figure 6. Core radius (bottom panel), central density (middle panel), and maximum acceleration of pulsar A (top panel) as a function of time in an *N*-body simulation that uses our best-fitting no-IMBH model as a starting point. Since NGC 6624 is in core collapse, the core radius and the central density show large fluctuations as the core contracts and re-expands due to the formation of binaries followed by heating due to encounters between cluster stars and these binaries. However, even during the strongest contraction phases the maximum $\dot{P}/P$ value of pulsar A is well below the observed value (shown by a blue line in the top panel). This implies that most of the observed period change of this pulsar is due to internal processes or a nearby companion, not the background cluster potential.

NGC 6624, two Galactic globular clusters that have been claimed to harbour IMBHs. Our results show that while IMBH models can be constructed that produce a simultaneous fit to the velocity and surface brightness profile of ω Cen, these models predict too many fast-moving stars within the central 20 arcsec of the cluster and can therefore be rejected. Instead, we find that a model containing 4.6 per cent of the cluster mass in a centrally concentrated cluster of stellar-mass black holes is a viable alternative to an IMBH model. This confirms earlier results by Zocchi et al. (2019). Such a model not only provides a very good fit to the velocity dispersion profile of ω Cen but also correctly predicts the velocity distribution of stars in the central 20 arcsec of ω Cen in the *HST* proper motion survey of Bellini et al. (2017). We find that a mass fraction of 4.6 per cent in stellar-mass black hole is compatible with the expected mass fraction due to stellar evolution of massive stars. Our *N*-body simulations show that this centrally concentrated cluster of black holes can have formed due to dynamical mass segregation and energy partition from an initially unsegregated distribution of stars.

For NGC 6624, we find that a model without an IMBH produces an excellent fit to the observed surface brightness and velocity dispersion profile as well as the stellar-mass function of the cluster, corroborating earlier results by Gieles et al. (2018). If an IMBH is present at all in this cluster, it must be less massive than 1000 M$_\odot$ since more massive IMBHs produce clusters that are in conflict with the observed surface brightness and velocity dispersion profile as well as the amount of mass segregation of NGC 6624. In particular, IMBHs with more than 5 per cent of the cluster mass (corresponding to more than about 3000 M$_\odot$) produce a strong central rise in velocity dispersion, which is seen neither in the *HST* proper motion dispersion profile of Watkins et al. (2015) nor in our radial velocity

dispersion profile. Hence, the observed period derivatives of the millisecond pulsars in the centre of NGC 6624 cannot be due to an acceleration produced by the smooth background potential of the cluster. Our results therefore show that caution has to be applied when using millisecond pulsars as probes of globular cluster potentials.

REFERENCES

Aarseth S. J., 1999, PASP, 111, 1333
Anderson J., van der Marel R. P., 2010, ApJ, 710, 1032
Barth A. J., Ho L. C., Rutledge R. E., Sargent W. L. W., 2004, ApJ, 607, 90
Baumgardt H., 2017, MNRAS, 464, 2174
Baumgardt H., Hilker M., 2018, MNRAS, 478, 1520
Baumgardt H., Hut P., Heggie D. C., 2002, MNRAS, 336, 1069
Baumgardt H., Makino J., Ebisuzaki T., 2004, ApJ, 613, 1143
Baumgardt H., Makino J., Hut P., 2005, ApJ, 620, 238
Baumgardt H., Hilker M., Sollima A., Bellini A., 2019, MNRAS, 482, 5138
Bekki K., Norris J. E., 2006, ApJ, 637, L109
Belczynski K., Kalogera V., Bulik T., 2002, ApJ, 572, 407
Belczynski K., Bulik T., Fryer C. L., Ruiter A., Valsecchi F., Vink J. S., Hurley J. R., 2010, ApJ, 714, 1217 (B10)
Bellini A. et al., 2014, ApJ, 797, 115
Bellini A., Anderson J., Bedin L. R., King I. R., van der Marel R. P., Piotto G., Cool A., 2017, ApJ, 842, 6
Bettwieser E., Sugimoto D., 1984, MNRAS, 208, 493
Castelli F., Kurucz R. L., 2004, preprint (arXiv:e-print)
Cooper M. C., Newman J. A., Davis M., Finkbeiner D. P., Gerke B. F., 2012, Astrophysics Source Code Library, record ascl:1203.003
Denissenkov P. A., Hartwick F. D. A., 2014, MNRAS, 437, L21
Dopita M., Hart J., McGregor P., Oates P., Bloxham G., Jones D., 2007, Ap&SS, 310, 255
Dopita M. et al., 2010, Ap&SS, 327, 245
Faber S. M. et al., 2003, in Iye M., Moorwood A. F. M., eds, Proc. SPIE Conf. Ser. Vol. 4841, Instrument Design and Performance for Optical/Infrared Ground-based Telescopes. SPIE, Bellingham, p. 1657
Farrell S. A., Webb N. A., Barret D., Godet O., Rodrigues J. M., 2009, Nature, 460, 73
Freire P. C. C. et al., 2011, Science, 334, 1107
Fryer C. L., 1999, ApJ, 522, 413
Fryer C. L., Belczynski K., Wiktorowicz G., Dominik M., Kalogera V., Holz D. E., 2012, ApJ, 749, 91 (F12)

Gebhardt K. et al., 2000, ApJ, 539, L13
Gerssen J., van der Marel R. P., Gebhardt K., Guhathakurta P., Peterson R. C., Pryor C., 2002, AJ, 124, 3270
Gieles M., Zocchi A., 2015, MNRAS, 454, 576
Gieles M., Balbinot E., Yaaqib R. I. S. M., Hénault-Brunet V., Zocchi A., Peuten M., Jonker P. G., 2018, MNRAS, 473, 4832
Giersz M., Leigh N., Hypki A., Lützendorf N., Askar A., 2015, MNRAS, 454, 3150
Gill M., Trenti M., Miller M. C., van der Marel R., Hamilton D., Stiavelli M., 2008, ApJ, 686, 303
Goldsbury R., Heyl J., Richer H., 2013, ApJ, 778, 57
Gray R. O., Corbally C. J., 1994, AJ, 107, 742
Gültekin K. et al., 2009, ApJ, 698, 198
Haggard D., Cool A. M., Heinke C. O., van der Marel R., Cohn H. N., Lugger P. M., Anderson J., 2013, ApJ, 773, L31
Harris W. E., 1996, AJ, 112, 1487
Husser T.-O. et al., 2016, A&A, 588, A148
Ibata R., Sollima A., Nipoti C., Bellazzini M., Chapman S. C., Dalessandro E., 2011, ApJ, 738, 186
Jalali B., Baumgardt H., Kissler-Patig M., Gebhardt K., Noyola E., Lützendorf N., de Zeeuw P. T., 2012, A&A, 538, A19
Ji J., Bregman J. N., 2013, ApJ, 768, 158
Jiang N. et al., 2018, ApJ, 869, 49
Johnson C. I., Pilachowski C. A., 2010, ApJ, 722, 1373
Kalirai J. S., Hansen B. M. S., Kelson D. D., Reitzel D. B., Rich R. M., Richer H. B., 2008, ApJ, 676, 594
Kamann S., Wisotzki L., Roth M. M., 2013, A&A, 549, A71
Kamann S. et al., 2018, MNRAS, 473, 5591
Kızıltan B., Baumgardt H., Loeb A., 2017, Nature, 542, 203
Kroupa P., 2001, MNRAS, 322, 231
Lin D. et al., 2018, Nature Astronomy, 2, 656
Miller M. C., Hamilton D. P., 2002, MNRAS, 330, 232
Milone A. P. et al., 2012, A&A, 540, A16
Mouri H., Taniguchi Y., 2002, ApJ, 566, L17
Newman J. A. et al., 2013, ApJS, 208, 5
Nitadori K., Aarseth S. J., 2012, MNRAS, 424, 545
Noyola E., Gebhardt K., 2006, AJ, 132, 447
Noyola E., Gebhardt K., Bergmann M., 2008, ApJ, 676, 1008
Nyland K., Marvil J., Wrobel J. M., Young L. M., Zauderer B. A., 2012, ApJ, 753, 103
Perera B. B. P. et al., 2017a, MNRAS, 468, 2114
Perera B. B. P. et al., 2017b, MNRAS, 471, 1258
Peuten M., Brockamp M., Küpper A. H. W., Kroupa P., 2014, ApJ, 795, 116
Portegies Zwart S. F., Baumgardt H., Hut P., Makino J., McMillan S. L. W., 2004, Nature, 428, 724
Pryor C., McClure R. D., Fletcher J. M., Hesser J. E., 1991, AJ, 102, 1026
Repetto S., Davies M. B., Sigurdsson S., 2012, MNRAS, 425, 2799
Saracino S. et al., 2016, ApJ, 832, 48
Servillat M., Farrell S. A., Lin D., Godet O., Barret D., Webb N. A., 2011, ApJ, 743, 6
Sollima A., Ferraro F. R., Bellazzini M., 2007, MNRAS, 381, 1575
Sollima A., Baumgardt H., Hilker M., 2019, MNRAS, 485, 1460
Spera M., Mapelli M., 2017, MNRAS, 470, 4739 (S17)
Spera M., Mapelli M., Bressan A., 2015, MNRAS, 451, 4086 (S15)
Strader J., Chomiuk L., Maccarone T. J., Miller-Jones J. C. A., Seth A. C., Heinke C. O., Sivakoff G. R., 2012, ApJ, 750, L27
Tonry J., Davis M., 1979, AJ, 84, 1511
Trager S. C., King I. R., Djorgovski S., 1995, AJ, 109, 218
Tremou E. et al., 2018, ApJ, 862, 16
Ulvestad J. S., Greene J. E., Ho L. C., 2007, ApJ, 661, L151
Usher C. et al., 2017, MNRAS, 468, 3828
van der Marel R. P., Anderson J., 2010, ApJ, 710, 1063
van Leeuwen F., Le Poole R. S., Reijns R. A., Freeman K. C., de Zeeuw P. T., 2000, A&A, 360, 472
VandenBerg D. A., Brogaard K., Leaman R., Casagrande L., 2013, ApJ, 775, 134
Watkins L. L., van der Marel R. P., Bellini A., Anderson J., 2015, ApJ, 803, 29

Webb N. A., Barret D., Godet O., Servillat M., Farrell S. A., Oates S. R., 2010, ApJ, 712, L107
Zocchi A., Gieles M., Hénault-Brunet V., 2017, MNRAS, 468, 4429
Zocchi A., Gieles M., Hénault-Brunet V., 2019, MNRAS, 482, 4713

SUPPORTING INFORMATION

Supplementary data are available at *MNRAS* online.

Table A1. DEIMOS stellar radial velocities for stars in the field of NGC 6624.

Please note: Oxford University Press is not responsible for the content or functionality of any supporting materials supplied by the authors. Any queries (other than missing material) should be directed to the corresponding author for the article.

APPENDIX: INDIVIDUAL RADIAL VELOCITIES OF STARS IN NGC 6624

See Tabe A1.

Table A1. DEIMOS stellar radial velocities for stars in the field of NGC 6624. The table gives the 2MASS ID, the right ascension and declination, the average heliocentric radial velocity and its 1σ error, the distance from the cluster centre, the 2MASS J- and K_S-band magnitudes, the membership probability based on the radial velocity and the number of radial velocity measurements. For stars with multiple radial velocity measurements, the probability that the star has a constant radial velocity is given in the final column. A full version of this table is available online.

2MASS ID	RA (J2000)	Dec. (J2000)	R_V (km s^{-1})	d (arcmin)	J (mag)	K_S (mag)	Prob. Mem.	N_{RV}	Prob. Single
18225355-3023248	275.723126	−30.390244	44.45 ± 2.95	616.74	13.95 ± 0.05	13.08 ± 0.06	0.106	1	
18225417-3022408	275.725745	−30.378021	-9.71 ± 3.41	602.72	11.51 ± 0.02	10.39 ± 0.03	0.000	1	
18225559-3020568	275.731659	−30.349119	-4.32 ± 4.30	582.91	12.78 ± 0.02	11.87 ± 0.02	0.000	1	
18225678-3021341	275.736596	−30.359499	-12.76 ± 2.46	565.99	11.94 ± 0.03	10.98 ± 0.03	0.000	1	
18234108-3022221	275.921187	−30.372812	50.58 ± 2.68	43.07	10.10 ± 0.02	8.90 ± 0.02	0.484	2	0.020
⋮	⋮	⋮	⋮	⋮	⋮	⋮	⋮	⋮	

This paper has been typeset from a TEX/LATEX file prepared by the author.